ADAPTIVE TIME DOMAIN BOUNDARY ELEMENT METHODS AND ENGINEERING APPLICATIONS

HEIKO GIMPERLEIN, MATTHIAS MAISCHAK AND ERNST P. STEPHAN

ABSTRACT. Time domain Galerkin boundary elements provide an efficient tool for the numerical solution of boundary value problems for the homogeneous wave equation. We review recent advances in their a posteriori error analysis and the resulting adaptive mesh refinement procedures, as well as basic algorithmic aspects of these methods. Numerical results for adaptive mesh refinements are discussed in 2 and 3 dimensions, as are benchmark problems in a half–space related to the transient emission of traffic noise.

1. Introduction. Efficient and accurate computational methods to simulate sound emission in space and time are of interest from the modeling of environmental noise to the acoustics of concert halls. This survey reviews time domain Galerkin boundary element methods for acoustic wave problems as studied particularly in [**16, 25, 26, 29, 42**], with references to related works. We particularly emphasise algorithmic aspects, recent progress towards space-time adaptive mesh refinements as well as applications to tire noise. Time domain boundary element methods prove to be stable and accurate in long–time computations and are competitive with frequency domain methods for realistic problems from the sound emission of tires.

Computations in time domain are of particular interest for problems beyond the reach of frequency domain methods, such as the simulation of transient dynamics, moving sound sources or nonlinear and dynamical contact problems. They can also be applied to obtain results in frequency domain, for all frequencies in one computation, with the help of the Fast Fourier Transform to translate between time and frequency.

This approach proves competitive if a broad band of frequencies is of interest.

Let $d = 2$ or 3 and $\Omega^i \subset \mathbb{R}^d$ be a bounded polygonal domain. For simplicity, we assume that the exterior domain $\Omega^e = \mathbb{R}^d \backslash \overline{\Omega^i}$ is connected and that the boundary $\Gamma = \partial\Omega$ is a Lipschitz manifold. Our emphasis will be on the case $d = 3$.

We aim to find a weak solution to an acoustic initial-boundary problem for the wave equation in Ω^e:

(1)
$$\frac{\partial^2 u}{\partial t^2} - \Delta u = 0 \quad \text{in } \mathbb{R}^+ \times \Omega^e$$
$$\frac{\partial u}{\partial n} - \alpha \frac{\partial u}{\partial t} = g \quad \text{on } \mathbb{R}^+ \times \Gamma$$
$$u(0, x) = \frac{\partial u}{\partial t}(0, x) = 0 \quad \text{in } \Omega^e \ .$$

Here n denotes the inward unit normal vector to $\partial\Omega^e$, g lies in a suitable Sobolev space, $\alpha \in L^\infty(\Gamma)$. In the case of an incoming wave u^{inc} scattered by Ω^i, the right hand side is $g = -\frac{\partial u^{inc}}{\partial n} + \alpha \frac{\partial u^{inc}}{\partial t}$. In order for (1) to be well-posed, α should have nonnegative real part, so that waves are not amplified at reflection. We also consider the simpler Dirichlet problem on Γ, for which instead of the absorbing boundary condition, $u|_{\mathbb{R}^+ \times \Gamma}$ is given.

For the boundary element methods discussed here, the acoustic and Dirichlet boundary problems are reformulated as time–dependent integral equations on $\mathbb{R}^+ \times \Gamma$. The integral equations are then numerically approximated by a Galerkin method in space–time. We present from [**25, 26**] an a priori and an a posteriori error analysis for methods based on integral formulations of the first kind. Computational experiments explore adaptive mesh refinements given in [**26**] and illustrate the methods for real–world problems from the sound emission of tires.

For the sound emission of tires, the wave equation also needs to be considered in a half space, $\Omega^i \subset \mathbb{R}^d_+$. The reader may wish to think of Ω^i as a solid tire, either in contact with the street (on $\partial\Omega^i \cap \partial\mathbb{R}^d_+$) or elevated above it $(\partial\Omega^i \cap \partial\mathbb{R}^d_+ = \emptyset$). We will concentrate on the latter case, as it simplifies notation. The boundary of $\Omega^e = \mathbb{R}^d_+ \backslash \overline{\Omega^i}$ decomposes into the boundary $\Gamma = \partial\Omega^e \cap \partial\Omega^i$ of the obstacle and the boundary $\Gamma_\infty = \partial\Omega^e \cap \partial\mathbb{R}^d_+$ of the half–space.

In this case the wave equation (1) is supplemented by acoustic boundary conditions on Γ_∞:

$$(2) \qquad \frac{\partial u}{\partial n} - \alpha_\infty \frac{\partial u}{\partial t} = 0 \quad \text{on } \mathbb{R}^+ \times \Gamma_\infty \ ,$$

where Re $\alpha_\infty \geq 0$ [**25**].

1.1. Related works. Hyperbolic time domain boundary integral equations and their numerical approximation go back to Friedman and Shaw [**24**], resp. Cruse and Rizzo [**18**]. The first modern boundary element methods and the basic algorithmic approaches were developed by Mansur [**38**], while the mathematical analysis of time dependent Galerkin boundary element methods was initiated by Bamberger and Ha-Duong [**11**]. Relevant works on the numerical implementation of the resulting marching-in-on-time scheme include the Ph.D. thesis of Terrasse [**49**] and [**21, 33**], which made the methods competitive for commercial applications.

As a main challenge in the stable implementation of time domain integral methods, the fundamental solution to the wave equation is singular, in odd dimensions a Dirac distribution supported on the light cone. The discretization and accurate computation of the entries in the Galerkin matrix has been considered in detail by Maischak, Ostermann and Stephan [**37, 47**], and one may refer to the dissertation of Ostermann [**42**] for further algorithmic details. See also [**8**] for an alternative approach.

The analysis initiated by Bamberger and Ha-Duong is based on an analysis in frequency domain. Using the Laplace transform to translate between frequency and time domain, well-posedness and convergence of numerical approximations can be analyzed for the infinite time interval $[0, \infty)$. Recent works by Aimi and collaborators [**3, 5, 6, 7**] emphasize formulations directly related to the conserved energy of the wave equation on a finite time interval $[0, T)$. At the expense of a slightly more involved weak formulation, the intrinsic coercivity directly implies the stability and convergence of these methods.

A detailed exposition of the mathematical background of time domain integral equations and their discretizations is available in the lecture notes by Sayas [**45**], see [**17, 32**] for more concise introductions and [**22**] for recent progress.

Recent interests have centered especially around fast methods, adaptivity and interface problems, including the coupling to finite elements with possibly different time discretizations. In particular, we mention the work of Sylvand on fast multipole methods [48]. First steps towards adaptive mesh refinements will be discussed in this article. They concern both space [26], time [44] and space-time in dimension 2 [29], but the optimal algorithmic implementation of these methods is only beginning to be understood.

For interface problems, Abboud, Joly, Rodriguez and Terrasse [1] initiated the mathematical analysis of FEM-BEM coupling in the time domain, coupling discontinuous finite elements to time domain integral equations. A subsequent work by Banjai, Lubich and Sayas [15] provides a fundamental general analysis of the coupling between different discretizations, including convolution quadrature. Energy-based formulations of FEM-BEM coupling have been investigated by Aimi and collaborators [2, 4], while the authors study adaptivity in the context of fluid-structure interaction [28]. Certain truly transient phenomena studied by engineers cannot be simulated in the frequency domain because they involve nonlinear contact and damage. See [34, 46] for time domain BEM approaches to such problems. Their mathematical analysis remains a hard challenge for future work.

In the engineering literature, fast methods are being developed and studied especially in the group of Eric Michielssen, see e.g. [52]. We finally mention the alternative ansatz functions in time that have been explored in [19, 20].

As an alternative to time domain boundary elements, the past years have seen rapid progress for convolution quadrature methods [13, 14, 45]. Convolution quadrature exploits the convolution structure in time of the integral equations to approximate them through the frequency domain by an inverse Laplace transform. Given a frequency domain solver, their implementation does not struggle with the careful, accurate computation of distributional integrals like time domain boundary elements. However, for long-time simulations and certain nonlinear problems with constraints, like dynamic contact and friction problems, the variational nature of Galerkin time domain methods may be advantageous.

Apart from wave propagation problems in $\mathbb{R}^d$, applications like

the sound emission and propagation above a street may naturally lead to problems posed in a half-space [16]. Here current work is motivated by the exact fundamental solutions obtained by Ochmann [41], as they allow acoustic Robin boundary conditions on the infinite boundary of the half-space. Further engineering applications involve wave propagation in moving coordinate systems or with moving sources [9, 43].

2. Boundary integral formulations. Similar to elliptic problems, the initial–boundary value problem (1) for the wave equation can be formulated as an integral equation of either the first or second kind on Γ.

We introduce the single layer potential in time domain as

$$S\varphi(t,x) = \int_{\mathbb{R}^+ \times \Gamma} G(t-\tau, x, y) \ \varphi(\tau, y) \ d\tau \ ds_y \ ,$$

where G is a fundamental solution to the wave equation. Specifically in 3 dimensions, it is given by

$$S\varphi(t,x) = \frac{1}{4\pi} \int_\Gamma \frac{\varphi(t-|x-y|, y)}{|x-y|} \ ds_y \ .$$

We similarly define the double-layer potential as

$$D\varphi(t,x) = \int_{\mathbb{R}^+ \times \Gamma} \frac{\partial G}{\partial n_y}(t-\tau, x, y) \ \varphi(\tau, y) \ d\tau \ ds_y \ .$$

For acoustic boundary conditions we require the single–layer operator V, its normal derivative K', the double–layer operator K and hypersingular operator W for $x \in \Gamma$, $t > 0$:

$$V\varphi(t,x) = 2 \int_{\mathbb{R}^+ \times \Gamma} G(t-\tau, x, y) \ \varphi(\tau, y) \ d\tau \ ds_y \, ,$$

$$K\varphi(t,x) = 2 \int_{\mathbb{R}^+ \times \Gamma} \frac{\partial G}{\partial n_y}(t-\tau, x, y) \ \varphi(\tau, y) \ d\tau \ ds_y,$$

$$K'\varphi(t,x) = 2 \int_{\mathbb{R}^+ \times \Gamma} \frac{\partial G}{\partial n_x}(t-\tau, x, y) \ \varphi(\tau, y) \ d\tau \ ds_y \, ,$$

$$W\varphi(t,x) = -2 \int_{\mathbb{R}^+ \times \Gamma} \frac{\partial^2 G}{\partial n_x \partial n_y}(t-\tau, x, y) \ \varphi(\tau, y) \ d\tau \ ds_y \ .$$

For the absorbing half-space, the single-layer potential S and boundary integral operators V, K, K', W are analogously defined in terms of an appropriate Green's function which satisfies the acoustic boundary condition (2) on Γ_∞. Explicit formulas have been obtained by Ochmann [40, 41], in particular for $d = 3$:

$$V\varphi(t,x) = \frac{1}{2\pi}\int_\Gamma \frac{\varphi(t - |x - y|, y)}{|x - y|}\, ds_y + \frac{1}{2\pi}\int_\Gamma \frac{\varphi(t - |x - y'|, y)}{|x - y'|}\, ds_y$$

$$- \frac{2\alpha_\infty}{\pi}\int_0^\infty \int_\Gamma \frac{\partial}{\partial s}\left[\frac{H(t - s - |x - y'|)}{\sqrt{(t - s + \alpha_\infty(x_3 + y_3))^2 + (\alpha_\infty^2 - 1)R^2}}\right]\varphi(s, y)\, ds_y\, ds\,.$$

Here, y' denotes the reflection of $y = (y_1, y_2, y_3) \in \Gamma$ on the street $\partial\mathbb{R}_+^3$: $y' = (y_1, y_2, -y_3)$. Furthermore, $R^2 = (x_1 - y_1)^2 + (x_2 - y_2)^2$, and H is the Heaviside function.

The boundary integral operators are considered between space–time anisotropic Sobolev spaces $H_\sigma^s(\mathbb{R}^+, \widetilde{H}^r(\Gamma))$. To define them, if $\partial\Gamma \neq \emptyset$, first extend Γ to a closed, orientable Lipschitz manifold $\widetilde{\Gamma}$.

On Γ one defines the usual Sobolev spaces of supported distributions:

$$\widetilde{H}^r(\Gamma) = \{u \in H^r(\widetilde{\Gamma}) : \operatorname{supp} u \subset \overline{\Gamma}\}\,, \qquad r \in \mathbb{R}\,.$$

Furthermore, $H^r(\Gamma)$ is the quotient space $H^r(\widetilde{\Gamma})/\widetilde{H}^r(\widetilde{\Gamma} \setminus \overline{\Gamma})$.
To write down an explicit family of Sobolev norms, introduce a partition of unity α_i subordinate to a covering of $\widetilde{\Gamma}$ by open sets B_i. For diffeomorphisms φ_i mapping each B_i into the unit cube $\subset \mathbb{R}^d$, a family of Sobolev norms is induced from $\mathbb{R}^d$:

$$\|u\|_{r,\omega,\widetilde{\Gamma}} = \left(\sum_{i=1}^p \int_{\mathbb{R}^d}(|\omega|^2 + |\xi|^2)^r|\mathcal{F}\left\{(\alpha_i u)\circ\varphi_i^{-1}\right\}(\xi)|^2 d\xi\right)^{\frac{1}{2}}\,.$$

The norms for different $\omega \in \mathbb{C}\setminus\{0\}$ are equivalent, and $\mathcal{F}$ denotes the Fourier transform. They induce norms on $H^r(\Gamma)$, $\|u\|_{r,\omega,\Gamma} = \inf_{v\in\widetilde{H}^r(\widetilde{\Gamma}\setminus\overline{\Gamma})}\|u + v\|_{r,\omega,\widetilde{\Gamma}}$, and on $\widetilde{H}^r(\Gamma)$, $\|u\|_{r,\omega,\Gamma,*} = \|e_+u\|_{r,\omega,\widetilde{\Gamma}}$. e_+ extends the distribution u by 0 from Γ to $\widetilde{\Gamma}$. It is stronger than $\|u\|_{r,\omega,\Gamma}$ whenever $r \in \frac{1}{2} + \mathbb{Z}$.

We now define a class of space–time anisotropic Sobolev spaces:

Definition 1. For $s, r \in \mathbb{R}$ define

$$H_\sigma^s(\mathbb{R}^+, H^r(\Gamma)) = \{u \in \mathcal{D}_+'(H^r(\Gamma)) : e^{-\sigma t}u \in \mathcal{S}_+'(H^r(\Gamma)) \text{ and } ||u||_{s,r,\Gamma} < \infty\} ,$$

$$H_\sigma^s(\mathbb{R}^+, \widetilde{H}^r(\Gamma)) = \{u \in \mathcal{D}_+'(\widetilde{H}^r(\Gamma)) : e^{-\sigma t}u \in \mathcal{S}_+'(\widetilde{H}^r(\Gamma)) \text{ and } ||u||_{s,r,\Gamma,*} < \infty\} .$$

$\mathcal{D}_+'(E)$ resp. $\mathcal{S}_+'(E)$ denote the spaces of distributions, resp. tempered distributions, on $\mathbb{R}$ with support in $[0, \infty)$, taking values in $E = H^r(\Gamma), \widetilde{H}^r(\Gamma)$. The relevant norms are given by

$$\|u\|_{s,r,\Gamma} = \left(\int_{-\infty+i\sigma}^{+\infty+i\sigma} |\omega|^{2s} \|\hat{u}(\omega)\|_{r,\omega,\Gamma}^2 \, d\omega \right)^{\frac{1}{2}} ,$$

$$\|u\|_{s,r,\Gamma,*} = \left(\int_{-\infty+i\sigma}^{+\infty+i\sigma} |\omega|^{2s} \|\hat{u}(\omega)\|_{r,\omega,\Gamma,*}^2 \, d\omega \right)^{\frac{1}{2}} .$$

For $|r| \leq 1$ the spaces are independent of the choice of α_i and φ_i. See [**25, 32**] for a more detailed discussion.

The representation formula uses S and D to express a solution to the wave equation in terms of its Dirichlet and Neumann data on Γ:

Theorem 1. *Let* $u \in L^2(\mathbb{R}^+, H^1(\Omega)) \cap H_0^1(\mathbb{R}^+, L^2(\Omega))$ *be the solution of* (1) *for a Lipschitz boundary* Γ. *Then*

$$u(t,x) = S\varphi(t,x) - Dp(t,x) ,$$

where $\varphi = [u]$ *is the jump of* u *across* Γ *and* $p = [\frac{\partial u}{\partial n}]$ *is the jump of the normal flux.*

As shown in [**33**] by reformulation to an interior problem, the initial boundary value problem (1) is equivalent to a system of integral equations of the first kind on Γ,

$$(3) \qquad \begin{cases} K'p - W\varphi + \alpha \frac{\partial \varphi}{\partial t} = F \\ p + \alpha(V\partial_t p + K\partial_t \varphi) = G . \end{cases}$$

Here, $\varphi = [u]$ and $p = [\frac{\partial u}{\partial n}]$ as above, and for an incoming wave u^{inc} scattered by Ω^i, we have $F = -2\frac{\partial u^{inc}}{\partial n}$ and $G = -2\alpha \frac{\partial u^{inc}}{\partial t}$. If $\alpha^{-1} \in L^\infty(\Gamma)$, we may pair these equations with test functions

$\partial_t \psi$ respectively $\frac{q}{\alpha}$, to obtain the following space-time variational formulation:

Find $\Phi = (\varphi, p) \in H^1_\sigma(\mathbb{R}^+, \widetilde{H}^{\frac{1}{2}}(\Gamma)) \times H^1_\sigma(\mathbb{R}^+, L^2(\Gamma))$ such that for all $\Psi = (\psi, q) \in H^1_\sigma(\mathbb{R}^+, \widetilde{H}^{\frac{1}{2}}(\Gamma)) \times H^1_\sigma(\mathbb{R}^+, L^2(\Gamma))$:

$$(4) \qquad a(\Phi, \Psi) = l(\Psi).$$

Here

$$(5) \qquad l(\Psi) = \int_0^\infty \int_\Gamma F \partial_t \psi \, ds_x \, d_\sigma t + \int_0^\infty \int_\Gamma \frac{Gq}{\alpha} \, ds_x \, d_\sigma t,$$

and $a(\Phi, \Psi)$ is given by

$$(6)$$
$$\int_0^\infty \int_\Gamma \left(\alpha (\partial_t \varphi)(\partial_t \psi) + \frac{1}{\alpha} pq + K' p (\partial_t \psi) - W \varphi (\partial_t \psi) + V (\partial_t p) q + K (\partial_t \varphi) q \right) ds_x \, d_\sigma t,$$

for $d_\sigma t = e^{-2\sigma t} dt$, $\sigma > 0$. The complementary Neumann problem, $\alpha = 0$, is discussed in [16, 27].

For the Dirichlet problem, a single-layer ansatz $u = 2S\phi$ leads to the integral formulation $V \partial_t \phi = \partial_t f$. Its variational formulation reads: Find $\phi \in H^1_\sigma(\mathbb{R}^+, \widetilde{H}^{-\frac{1}{2}}(\Gamma))$ such that

$$(7) \qquad b(\phi, \psi) = \langle \partial_t f, \psi \rangle \qquad \forall \psi \in H^1_\sigma(\mathbb{R}^+, \widetilde{H}^{-\frac{1}{2}}(\Gamma)),$$

where

$$b(\phi, \psi) = \int_0^\infty \int_\Gamma (V \partial_t \phi) \, \psi \, ds_x \, d_\sigma t,$$

$$\langle \partial_t f, \psi \rangle = \int_0^\infty \int_\Gamma (\partial_t f) \, \psi \, ds_x \, d_\sigma t.$$

Adapting fundamental observations in [11] and [32] to our situation, the bilinear forms $a(\Phi, \Psi)$ and $b(\phi, \psi)$ are continuous and, in a weak sense, coercive. They are related to the physical energy of the system. As a consequence, both the acoustic and the Dirichlet problem admit unique solutions for sufficiently smooth data. See [25] for details.

In addition to the variational formulations as integral equations of the first kind, for computations an integral equation of the second kind will prove useful. We will only state the Neumann case, $\alpha = 0$. Here a single-layer ansatz $u = S\varphi$ leads to the integral equation $(-I + K')\varphi = 2g$ and the weak formulation:

Find $\varphi \in H_{\sigma}^{\frac{1}{2}}([0,\infty), \widetilde{H}^{-\frac{1}{2}}(\Gamma))$ such that for all test functions $\psi \in H_{\sigma}^{\frac{1}{2}}([0,\infty), H^{-\frac{1}{2}}(\Gamma))$ there holds:

$$(8) \qquad \int_0^\infty \int_\Gamma (-I + K')\, \varphi\, \psi\; ds_x\, d_\sigma t = 2 \int_0^\infty \int_\Gamma g\, \psi\, ds_x\, d_\sigma t.$$

As it is equivalent to the original initial boundary value problem, also this formulation admits a unique solution for smooth right hand sides. However, while the integral equations of the first kind were related to the energy and coercive, this might not be the case for (8).

As written, the above integral equations (4), (7) and (8) formally hold both in the whole space $\mathbb{R}^d$ and the half space $\mathbb{R}_+^d$, with layer potentials defined in terms of the Green's function for the appropriate domain as above. The choice of the Green's function assures that even for the absorbing half–space we obtain an equation on Γ, not on the unbounded $\partial\Omega^e$.

3. Discretization. If Γ is not polygonal we approximate it by a piecewise polygonal curve resp. surface and write Γ again for the approximation. For simplicity, when $d = 3$ we will use here a surface composed of N triangular facets Γ_i such that $\Gamma = \cup_{i=1}^N \Gamma_i$. When $d = 2$, we assume $\Gamma = \cup_{i=1}^N \Gamma_i$ is composed of line segments Γ_i. In each case, the elements Γ_i are closed with $\text{int}(\Gamma_i) \neq \varnothing$, and for distinct Γ_i, $\Gamma_j \subset \Gamma$ the intersection $\text{int}(\Gamma_i) \cap \text{int}(\Gamma_j) = \varnothing$.

For the time discretization we consider a uniform decomposition of the time interval $[0,\infty)$ into subintervals $I_n = [t_{n-1}, t_n)$ with time step $|I_n| = \Delta t$, such that $t_n = n\Delta t$ $(n = 0, 1, \dots)$.
We choose a basis $\varphi_1^p, \cdots, \varphi_{N_s}^p$ of the space V_h^p of piecewise polynomial functions of degree p in space (continuous and vanishing at $\partial\Gamma$ if $p \geq 1$) and a basis $\beta^{1,q}, \cdots, \beta^{N_t,q}$ of the space $V_{\Delta t}^q$ of piecewise polynomial functions of degree of q in time (continuous and vanishing at $t = 0$ if $q \geq 1$).
Let $\mathcal{T}_S = \{T_1, \cdots, T_{N_s}\}$ be the spatial mesh for Γ and $\mathcal{T}_T = \{[0, t_1), [t_1, t_2), \cdots, [t_{N_t - 1}, T)\}$ the time mesh for a finite subinterval $[0, T]$.
We consider the tensor product of the approximation spaces in space and time, V_h^p and $V_{\Delta t}^q$, associated to the space–time mesh $\mathcal{T}_{S,T} =$

$\mathcal{T}_S \times \mathcal{T}_T$, and we write

$$V_{h,\Delta t}^{p,q} = V_h^p \otimes V_{\Delta t}^q \,.$$

These approximation spaces lead to Galerkin formulations for the acoustic and Dirichlet problems (4), (7) and (8). E.g. the Galerkin formulation of (7) reads: Find $\phi_{h,\Delta t} \in V_{h,\Delta t}^{p,q}$ such that

(9) $b(\phi_{h,\Delta t}, \psi_{h,\Delta t}) = \langle (\partial_t f)_{h,\Delta t}, \psi_{h,\Delta t} \rangle \qquad \forall \psi_{h,\Delta t} \in V_{h,\Delta t}^{p,q} \,.$

In [**25, 39**], we discuss a priori error estimates and the convergence of Galerkin approximations for (4) and (7) in a half space. Analogous results for the whole space and non-polygonal Γ date back to [**11**], in slightly different Sobolev norms. For the Dirichlet problem the basic estimate is the following:

Theorem 2 ([**25**]). *For the solutions $\phi \in H_\sigma^1(\mathbb{R}^+, \widetilde{H}^{-\frac{1}{2}}(\Gamma))$ of (7), $\phi_{h,\Delta t} \in V_{h,\Delta t}^{p,q}$ of (9) the following a priori estimate holds:*

$$\|\phi - \phi_{h,\Delta t}\|_{0,-\frac{1}{2},\Gamma,*} \lesssim \|(\partial_t f)_{h,\Delta t} - \partial_t f\|_{0,\frac{1}{2},\Gamma}$$

$$+ \inf_{\psi_{h,\Delta t} \in V_{h,\Delta t}^{p,q}} \left\{ (1 + \frac{1}{\Delta t})\|\phi - \psi_{h,\Delta t}\|_{0,-\frac{1}{2},\Gamma} + \frac{1}{\Delta t}\|\partial_t \phi - \partial_t \psi_{h,\Delta t}\|_{0,-\frac{1}{2},\Gamma} \right\} \,.$$

If in addition $\phi \in H_\sigma^s(\mathbb{R}^+, H^m(\Gamma))$, then

$$\|\phi - \phi_{h,\Delta t}\|_{0,-\frac{1}{2},\Gamma,*} \lesssim \|(\partial_t f)_{h,\Delta t} - \partial_t f\|_{0,\frac{1}{2},\Gamma}$$

$$+ \left((h^{\alpha_1} + \Delta t^{\beta_1})(1 + \tfrac{1}{\Delta t}) + (h^{\alpha_2} + \Delta t^{\beta_2})\tfrac{1}{\Delta t} \right) \|\phi\|_{s,m,\Gamma} \,,$$

where

$$\alpha_1 = m + \min\{\tfrac{1}{2}, -\tfrac{m}{2(m+s)}\}, \beta_1 = m + s + \min\{\tfrac{1}{2}, \tfrac{m+s}{2m}\},$$

$$\alpha_2 = m + \min\{\tfrac{1}{2}, -\tfrac{m}{2(m+s-1)}\}, \beta_2 = m + s + \min\{-\tfrac{1}{2}, -1 + \tfrac{m+s-1}{2m}\},$$

and $m \geq -\tfrac{1}{2}, s \geq 0.$

For the acoustic problem, we introduce the norm

$$\||p, \varphi\|| = \left(\|p\|_{0,0,\Gamma}^2 + \|\varphi\|_{0,\frac{1}{2},\Gamma,*}^2 + \|\partial_t \varphi\|_{0,0,\Gamma}^2 \right)^{\frac{1}{2}} \,.$$

Theorem 3 ([**25**]). *Assume (for simplicity) that $\alpha^{-1} \in L^\infty(\Gamma)$. For the solutions $\Phi = (p, \varphi) \in H^1_\sigma(\mathbb{R}^+, \widetilde{H}^{\frac{1}{2}}(\Gamma)) \times H^1_\sigma(\mathbb{R}^+, L^2(\Gamma))$ of (4) and $\Phi_{h,\Delta t} = (p_{h,\Delta t}, \varphi_{h,\Delta t}) \in V^{\tilde{p},\tilde{q}}_{h,\Delta t} \times V^{p,q}_{h,\Delta t}$ of its discretization the following a priori estimate holds:*

$$|||p - p_{h,\Delta t}, \varphi - \varphi_{h,\Delta t}|||$$
$$\lesssim ||F_{h,\Delta t} - F||_{0,0,\Gamma} + ||G_{h,\Delta t} - G||_{0,0,\Gamma}$$
$$+ \max\left(\frac{1}{\Delta t}, \frac{1}{\sqrt{h}}\right) \inf_{(q_{h,\Delta t}, \psi_{h,\Delta t}) \in V^{\tilde{p},\tilde{q}}_{h,\Delta t} \times V^{p,q}_{h,\Delta t}} \left(||p - q_{h,\Delta t}||_{1,0,\Gamma} + ||\varphi - \psi_{h,\Delta t}||_{1,\frac{1}{2},\Gamma}\right).$$

As for the Dirichlet problem, better estimates are obtained under smoothness assumptions, $\varphi \in H^{s_1}_\sigma(\mathbb{R}^+, H^{m_1}(\Gamma))$, $p \in H^{s_2}_\sigma(\mathbb{R}^+, H^{m_2}(\Gamma))$, [**25**].

We refer to [**27**] for an analysis of the Neumann problem. While computationally convenient, the analysis of numerical methods based on (8) remains open. In particular, schemes based on (8) are not known to be stable, or to admit unique discrete solutions.

4. A posteriori error estimates. Computable error indicators are a key ingredient to design adaptive mesh refinements. For time–dependent boundary element methods such efficient and reliable estimates of residual type have been obtained in [**26**], see also [**29, 30, 31**] and [**44**] for alternative error indicators and relevant estimates for the boundary integral operators. In the case of the Dirichlet problem we obtain in [**26**]:

Theorem 4 ([**26**]). *Let $\phi, \phi_{h,\Delta t} \in H^1_0([0,T], H^{-\frac{1}{2}}(\Gamma))$ be the solutions to (7) resp. (9). Assume that $R = \dot{f} - V\dot{\phi}_{h,\Delta t} \in H^0([0,T], H^1(\Gamma))$. Then*

$$||\phi - \phi_{h,\Delta t}||^2_{0,-\frac{1}{2},\Gamma} \lesssim ||R||_{0,1,\Gamma}\left(\Delta t ||\partial_t R||_{0,0,\Gamma} + ||h \cdot \nabla R||_{0,0,\Gamma}\right)$$
$$\lesssim \max\{\Delta t, h\}(||\partial_t R||_{L^2([0,T],L^2(\Gamma))} + ||\nabla R||_{L^2([0,T],L^2(\Gamma))})^2.$$

Remark 1. The estimate generalizes to arbitrary subspaces V in place of $V^{p,q}_{h,\Delta t}$, in particular discretizations with smooth ansatz functions in time are of interest [**44**].
a) As the single–layer potential maps $H^1([0,T], L^2(\Gamma))$ continuously to

$H^0([0,T], H^1(\Gamma))$, $V\dot{\phi}_{h,\Delta t}$ belongs to $H^0([0,T], H^1(\Gamma))$ if, for example, $\phi_{h,\Delta t} \in H^2([0,T], L^2(\Gamma))$. The a posteriori estimate is therefore only valid for sufficiently smooth discretizations, e.g. constructed from C^1–continuous splines.

b) In practice, we will here use $\Delta t \|\partial_t R\|_{0,0,\Gamma} + \|h \cdot \nabla R\|_{0,0,\Gamma}$ as an error indicator.

For the acoustic problem, a simple error estimate reads as follows:

Theorem 5 ([26]). *Let* $(\varphi, p), (\varphi_{h,\Delta t}, p_{h,\Delta t}) \in H_0^1([0,T], H^{\frac{1}{2}}(\Gamma)) \times H^1([0,T], L^2(\Gamma))$ *be the solutions to* (4) *and its discretized variant, and assume that*

$$R_1 = F - \alpha\dot{\varphi}_{h,\Delta t} + 2K'p_{h,\Delta t} - 2W\varphi_{h,\Delta t} \in L^2([0,T], L^2(\Gamma)) \ ,$$
$$R_2 = G + \alpha^{-1}p_{h,\Delta t} + 2V\dot{p}_{h,\Delta t} + 2K\dot{\varphi}_{h,\Delta t} \in L^2([0,T], L^2(\Gamma)) \ .$$

Then

$$|||p - p_{h,\Delta t}, \varphi - \varphi_{h,\Delta t}||| \lesssim \|R_1\|_{0,0,\Gamma} + \|R_2\|_{0,0,\Gamma} \ .$$

5. Algorithmic considerations. For piecewise constant test functions, the Galerkin discretization in space and time leads to a block–lower–triangular system of equations, which can be solved by blockwise forward substitution.

For example, the Dirichlet problem yields an algebraic system of the form

$$\sum_{m=1}^{n} V^{n-m} b^m = 2(f^{n-1} - f^n)$$

in time step $n = 1, 2, 3, \ldots$. It can be solved by forward substitution, giving rise to the *marching in on time* (MOT) scheme

$$V^0 b^n = 2(f^{n-1} - f^n) - \sum_{m=1}^{n-1} V^{n-m} b^m \ .$$

The Galerkin solution of (9) is then given by:

$$\dot{\varphi}_{h,\Delta t}(x,t) = \sum_{m=1}^{N_t} \sum_{i=1}^{N_s} b_i^m \beta^{m,0}(t)\varphi_i^p(x) \ .$$
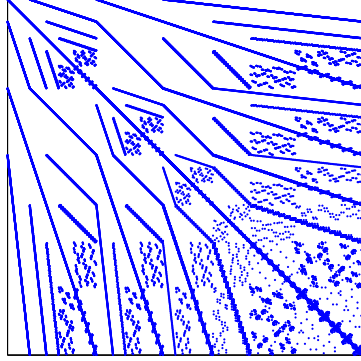
FIGURE 1. Sparsity pattern of the Galerkin matrix V^0 for a uniform discretization of the sphere [**42**].

The above fully discrete systems involve the computation of a series of matrices, that (if $\alpha_\infty = 0$) are sparsely populated, because the Dirac–delta fundamental solution restricts the number of interacting elements per time step. Figure 1 shows the distribution of nonzero matrix entries for a typical matrix V^0, when Γ is an approximation of S^2 by 5120 triangles. Note that the computation of each matrix only depends on the time difference. Furthermore, for bounded surfaces Γ the matrices V^{n-m} vanish whenever the time difference $l := n - m$ satisfies $l > \left[\frac{\text{diam}\,\Gamma}{\Delta t}\right]$, i.e. the light cone has traveled through the entire surface Γ.

5.1. An hp-composite quadrature of matrix elements. The most time consuming part in the MOT algorithm is the matrix computation, even though the resulting matrices are sparse in each time step. An efficient hp-composite Gauss-quadrature allows to compute the entries in V^l, and similarly for the other layer operators [**37, 42, 47**].

Recall the form of the matrix entries of V^l in $\mathbb{R}^3$ as an example:

$$\frac{1}{2\pi} \iiint_{\mathbb{R}^+ \times \Gamma \times \Gamma} \frac{\varphi_i^p(y)\partial_t \beta^{n,q}(t - |x - y|)}{|x - y|} \, \varphi_j^p(x)\beta^{m,q}(t) \, ds_y \, ds_x \, d_\sigma t \ .$$

First, the time integrals are evaluated analytically and result in an integration domain

$$E = \{(x,y) \in \Gamma \times \Gamma : r_{\min} \le |x - y| \le r_{\max}\}$$

of the form of a light cone, $r_{\min}$ and $r_{\max}$ depending on t_m and t_n. It remains to evaluate terms like

$$(10) \qquad G_{ij}^{\nu} = \iint\limits_{E} k_{\nu}(x - y)\varphi_i^p(y)\varphi_j^p(x)\, ds_y\, ds_x\,,$$

where $k_{\nu}(x - y) = |x - y|^{\nu}$ denotes a weakly singular kernel function. Our numerical quadrature separates the outer spatial integration from the singular inner one. Define the domain of influence of $x \in \mathbb{R}^3$ by

$$E(x) := B_{r_{\max}}(x) \setminus B_{r_{\min}}(x) = \{y \in \mathbb{R}^3 : r_{\min} \le |x - y| \le r_{\max}\}$$

as in Fig. 2(b). Fig. 2(a) similarly sketches the domain of influence of a triangle T,

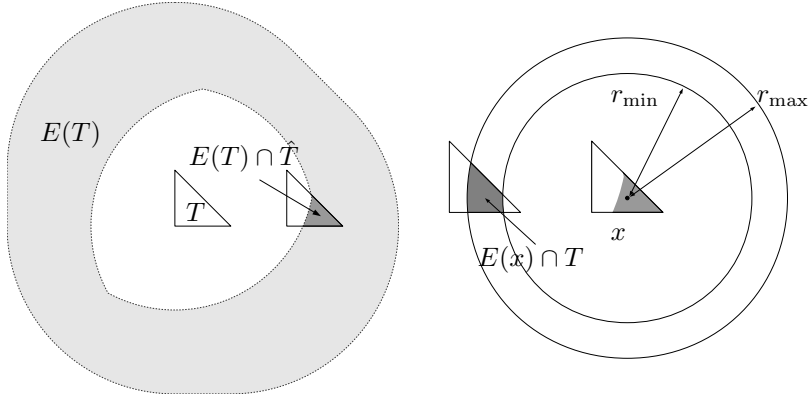$$E(T) := \bigcup_{x \in T} E(x) = \{y \in \mathbb{R}^3 : r_{\min} \le |x - y| \le r_{\max}\,,\ x \in T\}\,.$$

Defining $E(T_j, T_i) := E \cap (T_j \times T_i)$, we rewrite (10) as

$$G_{ij}^{\nu} = \sum_{\substack{T_{i'} \subset \operatorname{supp}\varphi_i \\ T_{j'} \subset \operatorname{supp}\varphi_j}} \iint\limits_{E(T_{j'}, T_{i'})} k_{\nu}(x - y)\varphi_i^p(y)\varphi_j^p(x)\, ds_y\, ds_x$$

$$= \sum_{\substack{T_{i'} \subset \operatorname{supp}\varphi_i \\ T_{j'} \subset \operatorname{supp}\varphi_j}} \int\limits_{T_{j'} \cap E(T_{i'})} \varphi_j^p(x) P_{i,i'}^p(x)\, ds_x\,,$$

with a retarded potential $P_{i,i'}$ given by

$$P_{i,i'}(x) := \int\limits_{E(x) \cap T_{i'}} k_{\nu}(x - y)\varphi_i^p(y)\, ds_y\,.$$

To simplify notation, we explain the quadrature for a simplified integral. Given triangles T, $\hat{T}$ and basis functions φ, $\widehat{\varphi}$ defined on

(a) Outer integral: Domain of influence of triangle $\hat{T}$ intersected with triangle T.

(b) Inner integral: Domain of influence $E(x)$ of point $x \in E(T) \cap \hat{T}$.

FIGURE 2. Domains of influence and the illumination of test and trial element $\widehat{T}$ and T during the evaluation of the inner and outer integral.

T and $\widehat{T}$, respectively, a typical entry in the Galerkin matrix reads
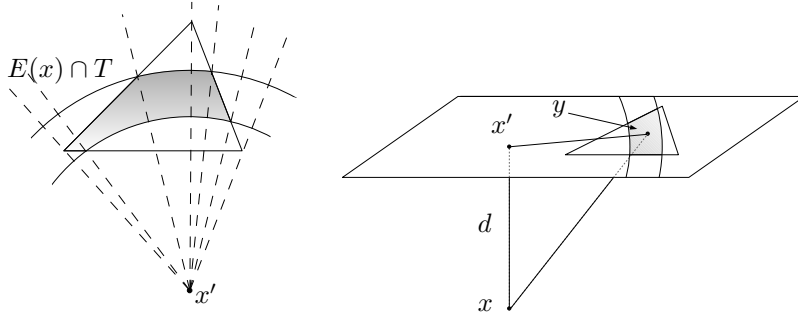
$$(11) \qquad \int_{E(T)\cap\widehat{T}} P\varphi(x)\widehat{\varphi}(x)\,ds_x\,, \quad P\varphi(x) := \int_{E(x)\cap T} k_\nu(x-y)\varphi(y)\,ds_y\,.$$

We evaluate the outer and the inner integral step by step decomposing the integration domain and using a grading strategy for the different singularities. It is crucial to take into account the cut-off behavior due to the different domains of influence, and below we recall the rigorous error analysis.

5.1.1. Composite inner quadrature. To calculate $P\varphi$ as defined in (11) first seek a parametric representation of $E(x) \cap T$. Let x' denote the orthogonal projection of x onto the triangle plane $\mathcal{E}_T$ and set $d := |x - x'|$, cf. Fig. 3(b). With $r'_{\min/\max} := (r^2_{\min/\max} - d^2)^{1/2}$, we have

$$E(x)\cap\mathcal{E}_T = (B_{r'_{\min}}(x') \setminus B_{r'_{\max}}(x'))\cap\mathcal{E}_T = \{y \in \mathcal{E}_T \ : \ r'_{\min} \le |x'-y| \le r'_{\max}\}\,,$$
$$E(x)\cap T = (B_{r'_{\min}}(x') \setminus B_{r'_{\max}}(x'))\cap T\,.$$

(a) Decomposition of $E(x) \cap T$ wrt. x' into $n_d = 5$ subelements. (b) Projection of x onto the triangle plane.

FIGURE 3

We introduce polar coordinates (r, θ) around x' and decompose

$$E(x) \cap T = \bigcup_{l=1}^{n_d} D_l, \quad D_l := \{(r, \theta) \, : \, \theta \in (\theta_l, \theta_{l+1}) \text{ and } r \in (r_{1,l}(\theta), r_{2,l}(\theta))\} \,,$$

where it can be shown that $n_d \leq 12$ and

$$r_{1,l} := \begin{cases} r'_{\min} & e \in B_{r'_{\min}(x)} \\ r_e(\theta) & \text{else} \end{cases} \,, \quad r_{2,l} := \begin{cases} r'_{\max} & e \notin B_{r'_{\max}(x)} \\ r_e(\theta) & \text{else} \end{cases} \,.$$

Here $r_e(\theta)$ is the parametrisation of the intersected triangle edge e in polar coordinates with respect to x'. In terms of the normal vector n of e and the end point v of e,

$$r_e(\theta) = \frac{v \cdot n}{n_1 \cos \theta + n_2 \sin \theta} \,.$$

Four generic cases of decomposition types are sketched in Fig. 4:

$$\hat{D}_1 := \{(r, \theta) \, : \, \theta \in (\theta_1, \theta_2) \text{ and } r \in (r_{\min}, r_{\max})\} \,,$$
$$\hat{D}_2 := \{(r, \theta) \, : \, \theta \in (\theta_1, \theta_2) \text{ and } r \in (r_{e_1}(\theta), r_{\max})\} \,,$$
$$\hat{D}_3 := \{(r, \theta) \, : \, \theta \in (\theta_1, \theta_2) \text{ and } r \in (r_{\min}, r_{e_2}(\theta))\} \,,$$
$$\hat{D}_4 := \{(r, \theta) \, : \, \theta \in (\theta_1, \theta_2) \text{ and } r \in (r_{e_1}(\theta), r_{e_2}(\theta))\} \,.$$
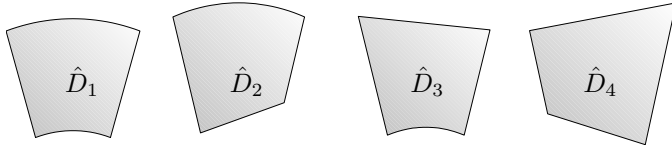
FIGURE 4. Generic integration domains

From (11) we obtain

$$P\varphi(x) = \sum_{l=1}^{n_d} \int_{\hat{D}_l} (d^2 + r^2)^{\frac{\nu}{2}} \varphi(r, \theta) r \, dr \, d\theta \, ,$$

where $d > 0$ and φ is sufficiently regular. For each of the domains $\hat{D}_l$, we can write the integral as

$$(12) \quad I^{(\hat{D}_l)} f := \int_{\theta_1}^{\theta_2} \int_{r_1(\theta)}^{r_2(\theta)} f(r, \theta) \, dr \, d\theta \, , \quad f(r, \theta) := (d^2 + r^2)^{\frac{\nu}{2}} \varphi(r, \theta) r.$$

To introduce our quadrature method, denote by $Q_n^{[a,b]} f := \sum_{i=1}^{n} w_i f(x_i)$ the Gauß-Legendre quadrature rule with n quadrature points to evaluate $\int_a^b f \, dx$. Given a subdivision of $[a, b]$ into m subintervals I_j, a variable order composite Gauß rule with degree vector $\mathbf{n} = (n_1, \ldots, n_m)$ is defined by $Q_{n,m,\sigma} f := \sum_{j=1}^{m} Q_{n_j}^{I_j} f$. We use a geometric subdivision of $[a, b]$ with m levels and grading parameter $\sigma \in (0, 1)$: $[a, b] = \bigcup_{j=1}^{m} I_j$, where for $j = 1, \ldots, m$ we let $I_j := [x_{j-1}, x_j]$, $x_0 := a$, $x_j := a + (b-a)\sigma^{m-j}$. For $n_r = (n_1^{(r)}, \ldots, n_m^{(r)})$, $m_r \geq 1$ and $\sigma_r \in (0, 1]$, the integral (12) is then computed as

$$Q^{\hat{D}_l} f := Q_{n_\theta}^{[\theta_1, \theta_2]} (Q_{n_r, m_r, \sigma_r}^{[r_1(\theta), r_2(\theta)]} f).$$

5.1.2. Error analysis for the evaluation of (12). A detailed analysis [42] shows that the integrand belongs to the countably normed, weighted space $B_\beta^0(T)$ of Babuska [10].

Definition 2 (Countably normed space $B_\beta^l(T)$)**.** We say $u \in B_\beta^l(T)$

with respect to a weight function $\Phi_{\beta,\alpha,l}$, if $u \in H^{l-1}(T)$ and if

$$\|\Phi_{\beta,\alpha,l}D^{\alpha}u\|_{L^2(\Omega)} \leq Cd^{|\alpha|-l}(|\alpha|-l)!$$

for $|\alpha| = l, l+1, \ldots$. Here the constants $C > 0$ and $d \geq 1$ are independent of $|\alpha|$.

If the number of angular quadrature points, n_θ, is chosen proportional to m_r, we obtain the following theorem on the accuracy of the quadrature in our TDBEM:

Theorem 6 ([**42**]). *Given a function $f \in B^0_\beta(T)$ with a weight function $\Phi_{\beta,\alpha,0}(r) = r^{|\alpha|+\beta}$ and let $\max(1, \sqrt{r_{max}})(\theta_2 - \theta_1) < eC_\theta$, then there holds for $\hat{D}_l$:*

$$|I^{(\hat{D}_l)}f - Q^{(\hat{D}_l)}f| \leq Ce^{-b\sqrt[3]{N}}$$

for $l = 1, \ldots, 4$. Here N denotes the total number of quadrature points and C and b are positive constants independently of N, but depending on the grading factor σ_r, the number of levels m_r and on f. Also,

$$C_\theta := \begin{cases} 1 & \text{for } \hat{D}_1 \\ \min_{\theta \in (\theta_1,\theta_2)} |\cos(\theta - \theta_1^*)| & \text{for } \hat{D}_2 \\ \min_{\theta \in (\theta_1,\theta_2)} |\cos(\theta - \theta_2^*)| & \text{for } \hat{D}_3 \\ \min_{\theta \in (\theta_1,\theta_2)} (|\cos(\theta - \theta_1^*)|, |\cos(\theta - \theta_2^*)|) & \text{for } \hat{D}_4, \end{cases}$$

and θ_i^* denotes the angle corresponding to the edge normal n_i, $i = 1, 2$.

6. Numerical experiments for tires. The numerical experiments in this section will use the discretization of the Neumann problem, (8) in $\mathbb{R}^3_+$, with $\alpha_\infty = 0$. It illustrates selected results from [**16**], for ansatz and test functions which are piecewise constant in space and time. For the computations we use $\sigma = 0$.

6.1. Validation on a problem with known solution. Considering a wave problem with known solution p in the exterior of a unit ball in $\mathbb{R}^3_+$ allows us to analyze the convergence properties of our method. For
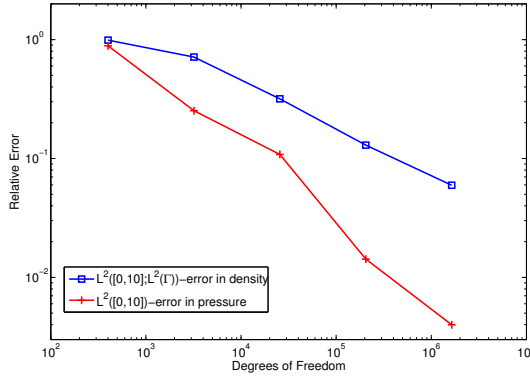
FIGURE 5. Relative L^2-errors of density $\varphi_{\Delta t,h}$ and pressure $p_{\Delta t,h}$ [16].

some fixed $0 < R < 1$, one obtains a radial pulse which solves (1) outside a unit sphere at a distance h above the street:

$$u(t,x) = \frac{r(h) - t}{2r(h)} \left[1 + \cos\left(\frac{\pi(r(h) - t)}{R} \right) \right] H(R - |r(h) - t|)$$
$$+ \frac{r(-h) - t}{2r(-h)} \left[1 + \cos\left(\frac{\pi(r(-h) - t)}{R} \right) \right] H(R - |r(-h) - t|).$$

Here, $H(t)$ denotes the Heaviside function and $r(h) = \|x_1, x_2, x_3 - h - 1\|$ and $r(-h) = \|x_1, x_2, x_3 + h + 1\|$. By a modification of [44] to the half-space, the density for the single layer potential ansatz is

$$(13) \quad \varphi(t,x) = -2 \sum_{k=0}^{\lfloor t/2 \rfloor} f_1(t - 2k) + 2 \sum_{k=0}^{\lfloor t/2 \rfloor} \int_{2k}^{t} e^{-(s-2k)} f_1(t - s)\, ds \ ,$$

where

$$f_1(t) = \left[\frac{t}{2r(h)^2} \left(1 + \cos\left(\frac{\pi(r(h) - t)}{R} \right) \right) - \frac{\pi}{R} \frac{r(h) - t}{2r(h)} \sin\left(\frac{\pi(r(h) - t)}{R} \right) \right]$$
$$\cdot H(R - |r(h) - t|).$$

Figure 4 shows the relative discretization errors

$$\frac{\|\varphi_{\Delta t,h} - \varphi\|_{L^2([0,10];L^2(\Gamma))}}{\|\varphi\|_{L^2([0,10];L^2(\Gamma))}} \quad \text{and} \quad \frac{\|u_{\Delta t,h}(t,x_0) - u(t,x_0)\|_{L^2([0,10])}}{\|u(t,x_0)\|_{L^2([0,10])}},$$

with $\varphi_{\Delta t,h}$ the TD-BEM Galerkin approximation of φ and $p_{\Delta t,h} = S\varphi_{\Delta t,h}$ on uniform meshes. Here $x_0 = (0,0,2.8)^\top$ for $R = 0.9$, $h = 0.63$. The figure shows a convergence rate of 0.4 for the density, resp. 0.65 for the sound pressure, with respect to the degrees of freedom (dof), i.e. the product of number of time steps and number of triangles. The ratio of the mesh size h and time step size Δt is $\Delta t/h \approx 0.38$.

6.2. Vibrating tire. Cyclic deformations of a moving tire enter the computations through the right hand side f in (8). Physically, the right hand side f is the result of the tire vibrations $f = -2\rho\frac{\partial^2 v_n}{\partial t^2}$. Here v_n describes the displacement of the tire in the outer normal direction and ρ the density of air. In [16] we determine f from the particle velocity $\frac{\partial u}{\partial \tau}$ on Γ, as supplied by the work group of W. Kropp at the Chalmers University in Gothenburg within the LeiStra3 cooperation. These particle velocities are given for 513 equidistant frequency points between 0Hz and 1809.4Hz in each of the 6027 nodes of the triangulation in Figure 6.

Figure 7 displays the A-weighted sound pressure level of the radiated acoustic wave. The simulation parameters are $\Delta t = 0.01$ averaged over 321 points in the hemisphere $\{x \in \mathbb{R}^3_+ : \|x\|_2 = 1\}$ [16]. These curves are obtained by a Fast Fourier Transform of the calculated sound pressure level for times $t \geq t_0$, with $t_0 = 0$, 0.005, and 0.02. The blue reference curve [51] is calculated by a Burton–Miller stabilized BEM collocation method for the Helmholtz equation with piecewise constant trial functions.

Further computational results in [16] for truck tires and the sound amplification in the horn geometry underline that the methods presented in this paper are competitive for industrial scale transient and broad–band frequency domain computations.

7. Adaptive mesh refinements. Fully space–time adaptive methods have been explored by M. Gläfke [29] for 2d problems. He does not treat the temporal domain separately from the spatial domain, but
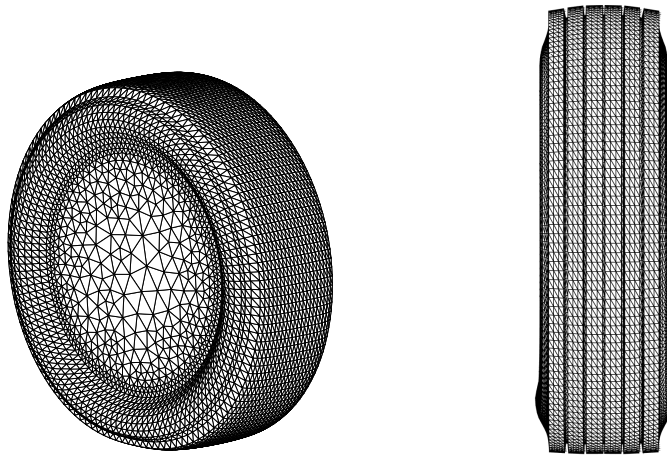
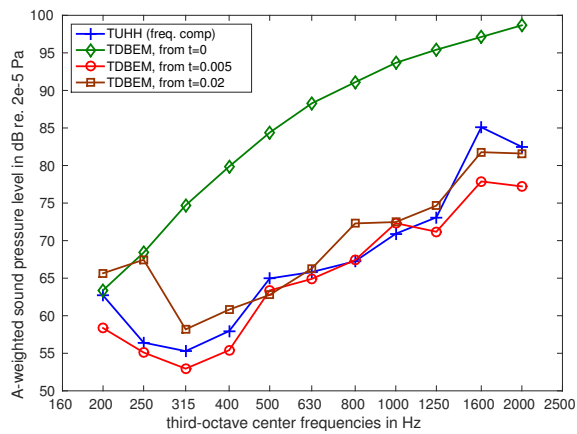FIGURE 6. Discretization of car resp. truck tires used for computations
[16].

FIGURE 7. Comparison of the A-weighted sound pressure level aver-
aged over 321 points and frequency bands for TDBEM and frequency
domain BEM [16].

refines the mesh of the space-time cylinder. More precisely, the rectan-
gular space-time elements are refined into four equally-sized rectangles.

The flexibility of this approach comes with additional computational cost: The MOT scheme no longer applies and one has to store and solve the full space-time system in one step.

Error indicators η such as from the a posteriori error estimates derived in Theorem 4 of Section 4 lead to an adaptive algorithm, based on the 4 steps

$$\textbf{SOLVE} \longrightarrow \textbf{ESTIMATE} \longrightarrow \textbf{MARK} \longrightarrow \textbf{REFINE}.$$

Space–time Adaptive Algorithm in 2d [29]:
Input: Mesh $\mathcal{T} = (\mathcal{T}_S \times \mathcal{T}_T)_0$, refinement parameter $\theta \in (0,1)$, tolerance $\epsilon > 0$, data f.

(1) Solve $V\dot{\varphi}_{h,\Delta t} = \dot{f}$ on $\mathcal{T}$.
(2) Compute the error indicators $\eta(\square)$ in each space-time rectangle.
(3) Stop if $\sum_i \eta^2(\square_i) < \epsilon^2$.
(4) Mark all $\square \in \mathcal{T}$ which satisfy refinement criterion based on θ.
(5) Refine each marked $\square$ into 4 new rectangles to obtain a new mesh $\mathcal{T}$
(6) Go to 1.

Output: Approximation of $\dot{\varphi}$.

In the following experiment, Gläfke uses a box pulse of the form $H(x_1 + x_2 + 2\alpha t + \lambda) - H(x_1 + x_2 + 2\alpha t)$ as the incident signal of the scattering problem with scatterer $[1,1]^2$. Here, $\lambda = 0.05$ and $\alpha = \frac{1}{\sqrt{2}}$. The box pulse is non-smooth, which appears to have an effect on the regularity of the solution of the problem: The convergence order for the adaptive version turns out to be genuinely higher than the one of the uniform version, even for large degrees of freedom. The meshes that result from the adaptive algorithm, as shown in Figure 8, are heavily refined along the part of the surface of the space-time cylinder where the box pulse moves along the scatterer.

Space–time adaptive methods in 3d, on the other hand, are still in their infancy. As a test case in [26] we concentrate on time–independent geometric singularities of the solution, e.g. in the horn geometry between the tire and the street. In this case we expect to
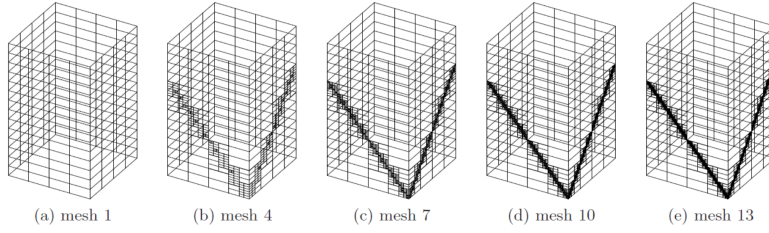
(a) mesh 1   (b) mesh 4   (c) mesh 7   (d) mesh 10   (e) mesh 13

FIGURE 8. Adaptive mesh refinements for a box pulse in 2d [29].

have time–independent meshes, refined near the singularities, which do not require an update of the Galerkin matrices in every time step.

From the discrete solution $\dot{\varphi}_{h,\Delta t}$ of the Dirichlet problem (9) and $\dot{f}$ we determine in every triangle $\triangle$ the time integrated local error indicator

$$\eta(\triangle)^2 = \int_0^T \int_\triangle [h \nabla_\Gamma (\dot{f} - V \dot{\varphi}_{h,\Delta t})]^2 \, ,$$

where the time integral is approximated by a Riemann sum.

The error indicators $\eta(\triangle)$ lead to

Adaptive Algorithm [26]:
Input: Mesh $\mathcal{T} = \mathcal{T}_0$, refinement parameter $\theta \in (0, 1)$, tolerance $\epsilon > 0$, data f.

(1) Solve $V \dot{\varphi}_{h,\Delta t} = \dot{f}$ on $\mathcal{T}$.
(2) Compute the error indicators $\eta(\triangle)$ in each triangle $\triangle \in \mathcal{T}$.
(3) Find $\eta_{max} = \max_\triangle \eta(\triangle)$.
(4) Stop if $\sum_i \eta^2(\triangle_i) < \epsilon^2$.
(5) Mark all $\triangle \in \mathcal{T}$ with $\eta(\triangle_i) > \theta \eta_{max}$.
(6) Refine each marked triangle into 4 new triangles to obtain a new mesh $\mathcal{T}$
   (and project the new nodes onto the sphere). Choose Δt such that $\frac{\Delta t}{\Delta x} \le 1$ for all traingles.
(7) Go to 1.

Output: Approximation of $\dot{\varphi}$.

According to the a posteriori estimates derived in [26], the error between the approximate and the actual solution to the problem is bounded by a multiple of ϵ, up to quantities involving time–derivatives of the residual $\dot{f} - V\dot{\varphi}_{h,\Delta t}$.

We consider the Dirichlet problem for the wave equation in the exterior of the three-dimensional (discretised) unit ball with a singular right hand side. We choose the right-hand side as $\dot{f}(t,x) = 2$ if $x_1 > 0$ and 0 otherwise. The function $\dot{f}$ is a toy example for a time–independent singularity, similar to the singular horn-like geometry where a tire meets a street (see [16]). We expect adaptive mesh refinements to concentrate around the line of discontinuity of $\dot{f}$, given by $x_1 = 0$. For simplicity we neglect the error of the surface approximation.

The numerical experiment depicted in Figure 9 shows the mesh generated by the above adaptive algorithm after three mesh refinements, starting with an initial icosahedral triangulation of the sphere with 80 nodes. Most refinements are near the discontinuity of f, as expected.

The above experiment presents only a first step towards space–time adaptive TDBEM, for the case of the geometric singularities relevant to sound radiation of tires. The optimal use of space–time adaptivity and its application to the acoustic boundary conditions remain to be explored.

8. Outlook. Engineering problems such as the sound emission of car and truck tires or scattering problems motivate the analysis of coupled finite and boundary elements. First works in this direction investigate the coupling of different time and spatial discretizations for scalar wave equations [1, 2, 4, 15]. Waves scattered by an immersed elastic object in a fluid provide a key example of practical interest. A basic well–posedness theory for the time–dependent problem can be found in [23, 36]. The a priori and a posteriori analysis of numerical discretizations based on Galerkin TDBEM [28], resp. convolution quadrature [35], has been recently considered.

For large–scale engineering computations, the efficient assembly of the space-time Galerkin matrix proves crucial. Fast multipole methods based on perturbative expansions of the Green's function in the far field are being developed especially by Sylvand [48], see also [12] for related work in the case of the Helmholtz-based convolution quadrature.
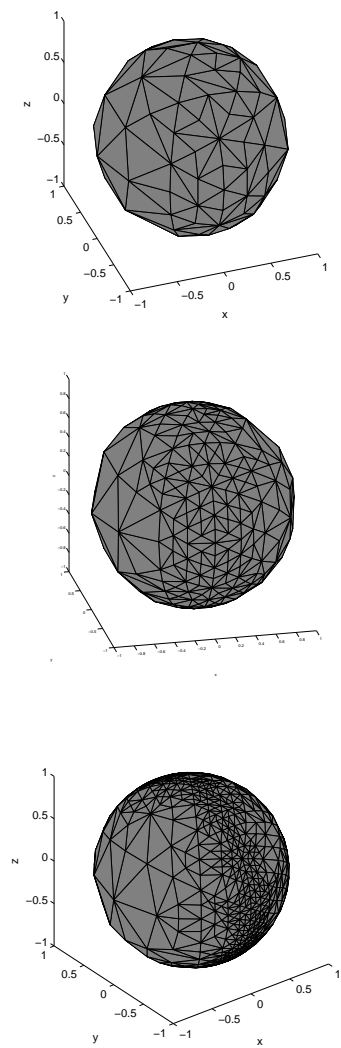
FIGURE 9. The first three adaptively generated meshes for $V\dot{\varphi} = \dot{f}$ starting from an icosahedral triangulation with 80 nodes, $\theta = 0.9$ [**26**].

In this article we provide a survey over recent advances in time domain boundary element methods for the wave equation and applications to engineering problems. The approach proves efficient and highly accurate for scattering and emission problems, and we demonstrate its relevance to applications in traffic noise. The a posteriori estimates presented in this survey lead to fast space-time adaptive mesh refinements. They make a first step towards high-order hp–adaptive methods in space and time.

REFERENCES

1. T. Abboud, P. Joly, J. Rodriguez, I. Terrasse, *Coupling discontinuous Galerkin methods and retarded potentials for transient wave propagation on unbounded domains*, J. Comp. Phys. **230** (2011), 5877–5907.

2. A. Aimi, M. Diligenti, A. Frangi, C. Guardasoni, *Energetic BEM-FEM coupling for wave propagation in 3D multidomains*, Internat. J. Numer. Methods Engrg. **97** (2014), 377–394.

3. A. Aimi, M. Diligenti, A. Frangi, C. Guardasoni, *Neumann exterior wave propagation problems: computational aspects of 3D energetic Galerkin BEM*, Comput. Mech. **51** (2013), 475–493.

4. A. Aimi, M. Diligenti, C. Guardasoni, S. Panizzi, *Energetic BEM-FEM coupling for wave propagation in layered media*, Commun. Appl. Ind. Math. textbf3 (2012), 418–438.

5. A. Aimi, M. Diligenti, A. Frangi, C. Guardasoni, *A stable 3D energetic Galerkin BEM approach for wave propagation interior problems*, Eng. Anal. Bound. Elem. **36** (2012), 1756–1765.

6. A. Aimi, M. Diligenti, C. Guardasoni, *On the energetic Galerkin boundary element method applied to interior wave propagation problems*, J. Comput. Appl. Math. **235** (2011), 1746–1754.

7. A. Aimi, M. Diligenti, C. Guardasoni, I. Mazzieri, S. Panizzi, *An energy approach to space-time Galerkin BEM for wave propagation problems*, Internat. J. Numer. Methods Engrg. **80** (2009), 1196–1240.

8. A. Aimi, M. Diligenti, C. Guardasoni, *Numerical integration schemes for the Galerkin BEM related to wave propagation problems*, Quaderni Dip. Mat. Univ. Parma. **495**, 1–34.

9. H. Antes, J. Baaran, *Noise radiation from moving surfaces*, Engineering Analysis with Boundary Elements **25** (2001), 725–740.

10. I. Babuska, B. Q. Guo, *Regularity of the solution of elliptic problems with piecewise analytic data. I. Boundary value problems for linear elliptic equation of second order*, SIAM J. Math. Anal. **19** (1988), 172–203.

11. A. Bamberger, T. Ha Duong, *Formulation variationnelle espace-temps*

pour le calcul par potentiel retard de la diffraction d'une onde acoustique, Math. Meth. Appl. Sci. **8** (1986), 405–435 and 598–608.

12. L. Banjai, M. Kachanovska, *Fast convolution quadrature for the wave equation in three dimensions*, J. Comp. Phys. **279** (2014), 103–126.

13. L. Banjai, S. Sauter, *Rapid solution of the wave equation in unbounded domains*, SIAM J. Numer. Anal. **47** (2008/09), 227–249.

14. L. Banjai, M. Schanz, *Wave propagation problems treated with convolution quadrature and BEM*. In: Lect. Notes Appl. Comput. Mech. **63**, Fast boundary element methods in engineering and industrial applications, Springer, 2012, pp. 145–184.

15. L. Banjai, C. Lubich, F.-J. Sayas, *Stable numerical coupling of exterior and interior problems for the wave equation*, Numer. Math. **129** (2015), 611–646.

16. L. Banz, H. Gimperlein, Z. Nezhi, E. P. Stephan, *Time domain BEM for sound radiation of tires*, Comput. Mech. **58** (2016), 45–57.

17. M. Costabel, *Time-dependent problems with the boundary integral equation method*. In Encyclopedia of Computational Mechanics, E. Stein, R. de Borst, and J. R. Hughes, Eds. John Wiley & Sons, Chichester, 2004, pp. 703-721.

18. T. A. Cruse, F. J. Rizzo, *A direct formulation and numerical solution of the general transient elastodynamic problem I*, J. Math. Analysis Appl. 22 (1968), 244–259.

19. P. J. Davies, D. B. Duncan, *Convolution-in-time approximations of time domain boundary integral equations*, SIAM J. Sci. Comput. **35** (2013), B43–B61.

20. P. J. Davies, D. B. Duncan, *Convolution spline approximations for time domain boundary integral equations*, J. Integral Equations Applications **26** (2014), 369–412.

21. Y. Ding, A. Forestier, T. Ha Duong, *A Galerkin scheme for the time domain integral equation of acoustic scattering from a hard surface*, J. Acoust. Soc. Am. **86** (1989), 1566–1572.

22. C. L. Epstein, L. Greengard, T. Hagstrom, *On the stability of time domain integral equations for acoustic wave propagation*, Discr. Continuous Dynamical Syst. **36** (2016), 4367–4382.

23. M. Filipe, *Etude mathematique et numerique d'un probleme d'interaction fluide–structure dependant du temps par la methode de couplage elements finis – equations integrals*, Ph.D. thesis, Ecole Polytechnique, 1994.

24. M. Friedmann, R. Shaw, *Diffraction of pulses by cylindrical obstacles of arbitrary cross section*, J. Appl. Mech. 29 (1962), 40–46.

25. H. Gimperlein, Z. Nezhi, E. P. Stephan, *A priori error estimates for a time-dependent boundary element method for the acoustic wave equation in a half-space*, Math. Meth. Appl. Sci., special issue, online first (2014), doi: 10.1002/mma.3340.

26. H. Gimperlein, Z. Nezhi, C. Özdemir, E. P. Stephan, *A residual a posteriori error estimate for the time domain boundary element method*, preprint.

27. H. Gimperlein, C. Özdemir, E. P. Stephan, *Time domain boundary element methods for the Neumann problem and sound radiation of tires*, preprint.

28. H. Gimperlein, E. P. Stephan, *Analysis of a time–dependent FEM/BEM coupling method for fluid–structure interaction*, in preparation.

29. M. Gläfke, *Adaptive Methods for Time Domain Boundary Integral Equations*. Ph.D. thesis, Brunel University, 2012.

30. M. Gläfke, M. Maischak, *Regularity of 2D time domain boundary integral operators*, preprint.

31. M. Gläfke, M. Maischak, *Wave-number explicit generalised mapping properties for Helmholtz boundary integral operators , applied to time domain boundary integral operators*, preprint.

32. T. Ha Duong, *On retarded potential boundary integral equations and their discretizations*, in: Topics in computational wave propagation, pp. 301–336, Lect. Notes Comput. Sci. Eng., **31**, Springer, Berlin, 2003.

33. T. Ha Duong, B. Ludwig and I. Terrasse, *A Galerkin BEM for transient acoustic scattering by an absorbing obstacle*, Internat. J. Numer. Methods Engrg. **57** (2003), 1845–1882.

34. G. D. Hatzigeorgiou, D. E. Beskos, *Dynamic inelastic structural analysis by the BEM: A review*, Engineering Analysis with Boundary Elements **35** (2011), 159–169.

35. G. C. Hsiao, T. Sanchez-Vizuet, F.-J. Sayas, *Boundary and coupled boundary-finite element methods for transient wave-structure interaction*, preprint.

36. G. C. Hsiao, F.-J. Sayas, R. J. Weinacht, *Time-dependent fluid-structure interaction*, Math. Meth. Appl. Sci., special issue, online first (2015), doi: 10.1002/mma.3427.

37. M. Maischak, E. Ostermann, E. P. Stephan, *TD-BEM for Sound Radiation in three Dimensions and the Numerical Evaluation of Retarded Potentials*, International Conference on Acoustics, NAG/DGA. 2009.

38. W. J. Mansur, *A time-stepping technique to solve wave propagation problems using the boundary element method*, Ph.D. thesis, University of Southampton, 1983.

39. Z. Nezhi, *Adaptive Time Domain Boundary Element Method for Sound Radiation of tires*, Ph.D. thesis, Leibniz Universität Hannover, 2014.

40. M. Ochmann, *The complex equivalent source method for sound propagation over an impedance plane*, J. Acoust. Soc. Am. **116** (6), 2004.

41. M. Ochmann, *Closed form solutions for the acoustical impulse response over a masslike or an absorbing plane*, J. Acoust. Soc. Am. **129** (6), 2011.

42. E. Ostermann, *Numerical Methods for Space-Time Variational Formulations of Retarded Potential Boundary Integral Equations*, Ph.D. thesis, Leibniz Universität Hannover, 2009.

43. K. M. Rasmussen, S. R. K. Nielsen, P. H. Kirkegaard, *Boundary element method solution in the time domain for a moving time-dependent force*, Computers and Structures **79** (2001), 691–701.

44. S. Sauter, A. Veit, *Adaptive time discretization for retarded potentials*, Numer. Math. **132** (2016), 569–595.

45. F.-J. Sayas, *Retarded Potentials and Time Domain Boundary Integral Equations: a road-map*, Springer Series in Comp. Math. 50, Springer, 2016.

46. G. E. Stavroulakis, H. Antes, P. D. Panagiotopoulos, *Transient elastodynamics around cracks including contact and friction*, Computer Methods in Applied Mechanics and Engineering **177** (1999), 427–440.

47. E. P. Stephan, M. Maischak, E. Ostermann, *Transient boundary element method and numerical evaluation of retarded potentials*, Computational Science–ICCS 2008 2008.

48. G. Sylvand, *La Methode Multipole Rapide en Electromagnetisme: Performances, Parallelisation, Applications*, Ph.D. thesis, Ecole Nationale des Ponts et Chaussees, 2002.

49. I. Terrasse, *Résolution mathématique et numérique des équations de Maxwell instationnaires par une méthode de potentiels retardés*, Ph.D. thesis, École Polytechnique, Palaiseau, 1993.

50. A. Veit, *Numerical methods for the time domain boundary integral equations*, Ph.D. thesis, Universität Zürich, 2011.

51. O. von Estorff et al., *Abschlussbericht SPERoN 2020 – Teil II, Entwicklung einen performanten Rechenmodells zur Berechnung und Reduzierung der Geruschabstrahlung von Reifen*, 2014.

52. A. E. Yilmaz, J.-M. Jin, E. Michielssen, *Time domain adaptive integral method for surface integral equations*, IEEE Trans. Antennas Propagation **52** (2004) 2692–2708.

Maxwell Institute for Mathematical Sciences and Department of Mathematics, Heriot-Watt University, Edinburgh EH14 4AS, United Kingdom, and Institute for Mathematics, University of Paderborn, Warburger Str. 100, 33098 Paderborn, Germany
Email address: **h.gimperlein@hw.ac.uk**

Department of Mathematics, Brunel University, Uxbridge, UB8 3PH, United Kingdom
Email address: **matthias.maischak@brunel.ac.uk**

Institute of Applied Mathematics, Leibniz University Hannover, 30167 Hannover, Germany
Email address: **stephan@ifam.uni-hannover.de**